Image Processing in the Tracking and Analysis of Red Blood Cell Motion in Micro-Circulation Experiments

Ana João and Alberto Gambaruto

Abstract Red blood cells constitute about 45 % of the blood cells and contain haemoglobin which facilitates transportation of oxygen. Even though RBCs usually present shapes similar to circular cushions with a dimple on the side, they can, sometimes, deform into an asymmetrical slipper shape. As RBCs are required to flow through thin capillaries to deliver oxygen to the human body, deformability is crucial when studying microcirculation. By studying their behaviour in blood vessels one can analyse the normal state of these cells and the diseased states. The insights can help to understand the mechanisms involved in arterial disease and other blood flow related conditions. The aim of this work is to analyse RBC behaviour in experimental conduits using image-based techniques. Images were acquired from a micro-channel with a contraction, where the red blood cells experience shear flow near the center-line. RBCs are tracked throughout a digital video sequence and analysed in terms of shape and deformation index at different time frames. Results show that under strong flows, RBC present an extremely deformable behaviour. RBC tracking and image processing techniques are implemented and analysed.

1 Introduction

The cardiovascular system is vitally important, responsible largely for the transport of nutrients and waste products, but also in the transport of heat, chemical triggers and also responsible for protection, such as healing wounds through thrombus formation, the transport of white blood cells and many other phenomena. The blood acts as the medium for the transport, and is composed largely of plasma,

A. João (✉) · A. Gambaruto
Departamento de Matemática and CEMAT/IST, Instituto Superior Técnico,
Technical University of Lisbon, Av. Rovisco Pais 1, 1049-001 Lisbon, Portugal
e-mail: ana.joao@ist.utl.pt

R. Lima et al. (eds.), *Visualization and Simulation of Complex Flows in Biomedical Engineering*, Lecture Notes in Computational Vision and Biomechanics 12,
DOI: 10.1007/978-94-007-7769-9_8,

with a suspension mainly of red blood cells (RBCs), white blood cells and platelets. The state of the blood is therefore an important indicator to the health of an individual (Fung et al. 1970). During the past years, the rapid growth of biomedical technology, mainly of cardiovascular devices and blood-analysis devices has stimulated research on blood degradation and thrombosis associated with their use. The importance of checking the health state of whole blood has stimulated for faster, cheaper and more compact devices for analysis. Great part of the research performed has been focused on red blood cells, which have high concentrations in blood ($\sim$45 %) and carry high concentrations of oxygen.

Discoveries that normal erythrocytes are nucleus free deformable liquid capsules, enclosed by a biological membrane, which are almost incompressible and show quasi-elastic response to shear and bending deformation, have led to numerous experimental and computational studies. The majority of these studies focus on two goals: firstly, explain the biconcave shape of healthy red blood cells (RBCs) and evaluate whether its membrane is stressed while in resting configuration; secondly, to describe the RBCs behavior in large scale and capillary blood flow (Mohandas and Evans 1994).

RBCs typically have an average diameter of 7–9 μm at rest, but undergo large deformability when submitted to certain flow conditions. RBC deformation is an important property of oxygen delivery to the body and the passage in small vessels such as capillaries. The deformation of RBCs is also responsible for the non-Newtonian rheology of blood. A decrease in RBC deformation (as is caused by malaria infection) will have serious consequences and may lead to serious health problems (Hou et al. 2010).

Studies have suggested that a minimum RBC deformability may be connected to certain diseases and therefore analysis of RBC deformation can be a crucial tool for medical diagnosis (Hou et al. 2010). The majority of research on human RBC deformation has been performed using a variety of techniques, such as optical tweezers or micro-pipeting. Even though these techniques involve both shear and extension, most of the works usually focus on shear effects on RBCs (Musielak 2009).

Here we study the deformation of RBCs in an experimental setup, of a micro-channel with a sudden change in cross-sectional area in the geometry, through image processing and tracking. The experimental data has been kindly made available from Prof Rui Lima and Prof. Takami Yamaguchi, and their research teams at Instituto Politécnico de Bragança and Tohoku University, respectively. The data obtained from the experiments is a digital video sequences captured with the following characteristics: sample rate of 8,000 pps, exposure time 6 μs, image interval 125 μs, and magnification 60×, equivalent to a pixel size of 2.7 μm. For image analysis purposes, the captured video was converted to a stack of images, with resolution of 208 × 800. The micro-channel used was produced in poly-dimethylsiloxane (PDMS) using standard soft-lithography techniques from a SU-8 photoresist mold.

The different stages of the study of the images are, in order: filtering, contrast enhancement, segmentation and finally tracking and analysis. These stages are detailed in the following sections. For simplicity, selected representative images

from the stack are used in order to highlight the processing stage, with the intention that the discussion carries naturally to the entire set of images used. As a initial step, the stack of images was averaged and removed from each individual image; removing therefore some impurity (such as spots due to dirt) and especially the channel geometry, in this manner giving emphasis to the RBCs.

2 Image Preprocessing

2.1 Image Filtering

Prior to segmentation of the RBCs and the analysis of their motion and shape, the images are processed in order to improve their interpretation. Common procedures consist of filtering (de-noising) the images, followed by contrast enhancement to recapture smoothed features. In certain occasions optimal results are seen in procedures to first improve the contrast and them perform filtering, however this is not the common practice.

Images are often diminished by noise and artefact. In microscopy, noise can be seen as the systematic or random corruption of single or small cluster of pixels. Artefacts include RBCs moving in and out of the focal plane that results in a fading and smearing of the RBC definition as well as reduction in cross-sectional area, and partial volume effects. Noise can be understood as an undesired signal that affects the communication or measurement of another signal. Artefacts, on the other hand, are errors in representation of visual information caused by the imaging equipments and modalities. By reducing the noise intensity in the image a clearer and more robust interpretation is possible. A number of approaches have been proposed for image de-noising, such as low-pass filtering using a Fourier (or wavelet) expansion or simply a convolution to a Gaussian (hence, the solution to the heat equation). Here we briefly discuss the background and motivation for adopting a partial differential equation based diffusion, that is in essence an anisotropic diffusion equation, such that the diffusion will occur in rather homogeneous regions and not across boundaries (Perona and Malik 1990).

Let us consider each image of the stack as 2-dimensional orthogonal domain $\Omega = (1, N_1) \times (1, N_2)$. Considering $I_0(x, y, 0)$ to be the original image, we denote as the image $I(x, y, t)$ at a moment during the processing phase. The non-linear anisotropic diffusion process proposed by Perona and Malik in (Perona and Malik 1990) looks for the solution of

$$\frac{\partial I(x, y, t)}{\partial t} = \nabla \cdot (c(x, y, t) \nabla I(x, y, t)) \tag{1}$$

where the diffusion coefficient is commonly a decreasing function of the image gradient $c(x, y, t) = g(|\nabla I(x, y, t)|)$; $\nabla\cdot$ and ∇ are the divergence and the gradient operator, respectively. The anisotropic diffusion coefficient is a chosen to estimate

edges in the object, since these will have the largest gradient in the image. A popular choice is

$$g(|\nabla I(x,y,t)|) = \frac{1}{1+|\nabla I|^2/K^2} \tag{2}$$

hence at edges the diffusion coefficient is small and large in region of rather homogeneous intensity. This form of the equation is denoted by *PM* [from the work of Perona and Malik (Perona and Malik 1990)] in the following discussion of the filtering performance.

If in Eq. (1) the diffusion coefficient is made constant, it reduces to the well known heat equation $\frac{\partial I(x,y,t)}{\partial t} = c\nabla^2 I(x,y,t)$. Expanding Eq. (1) with $c = g(|\nabla I|)$ we obtain

$$I_t = g(|\nabla I|)\partial_{\tau\tau} I + [g(|\nabla I|) + 2|\nabla I|^2 g'(|\nabla I|)]\partial_{vv} I \tag{3}$$

where τ and v are orthogonal direction tangential and normal to an edge. Hence the diffusion process is decomposed into a process tangential to an edge and normal to it. The coefficient of the derivative in the direction normal to the level set of I becomes negative for large values of the image gradient ("edges" in an image) and popular choice of g mentioned above (Guidotti 2012). This leads to a regime where diffusion can reverse its sign at least in one direction, and hence a forward–backward diffusion process is obtained. The Perona-Malik equation given in Eq. (1) is ill-posed and several approaches have been proposed to regularise the equations (Guidotti 2012). In practice however the approach work well and observed problems are occasional staircasing effects after long time evolution, and in other words a mild gradient region evolves into piece-wise almost linear segments separated by jumps. The original image used through out the analysis can be seen in Fig. 1.

An alternative approach is to define the image edge not by the gradient of the image but the Laplacian of the image. This can be seen to be appropriate in the case of a slowly varying edge with a constant gradient along it: the edge will have the same gradient and hence no sharpening effect will be produced, while using a diffusion coefficient based on the Laplacian will provide a more appropriate edge detection criterion. This is the case in RBCs visualisation using confocal microscopy as the light distortion due to the membrane covers several pixels, hence indicating that the edge is represented by a uniform change in the image (constant image gradient) over a spatial extent of a few pixels. Gilboa et al. (Gilboa et al. 2004) combined the diffusion equation with the Schrödinger equation such that the non-linear complex diffusion process is given by

$$\frac{\partial}{\partial t} I = \nabla \cdot (d(\mathrm{Im}(I)\ \nabla I) \tag{4}$$

where $\mathrm{Im}(\cdot)$ denotes the imaginary value and the diffusion coefficient is defined as

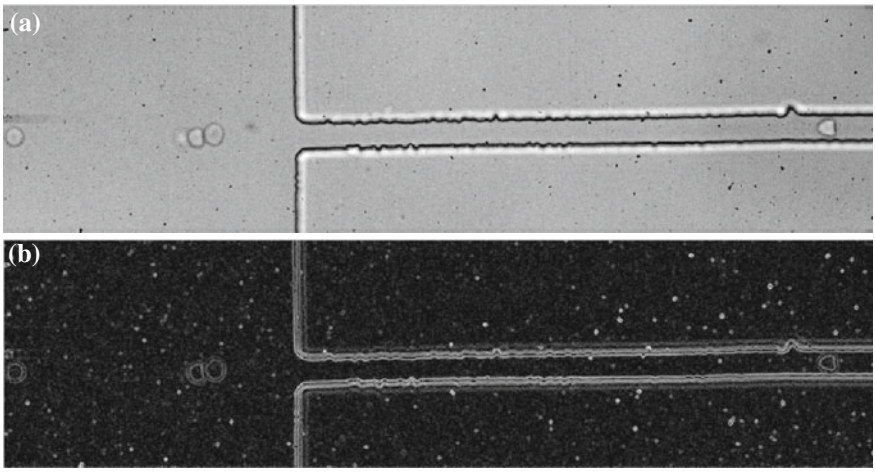

Fig. 1 **a** Original image (frame 50)—PMDS hyperbolic microchannel, **b** Image gradient

$$d(\mathrm{Im}(I) = \frac{\exp(i\theta)}{1 + \left(\frac{\mathrm{Im}(I)}{k\theta}\right)^2} \approx \frac{1}{1 + \left(\frac{\Delta I}{\kappa}\right)^2} \tag{5}$$

It has been reported in (Gilboa et al. 2004) that $\mathrm{Im}(I)$ approximates a smoothed second order derivative of the image (Salinas and Fernandez 2007). This avoids the discretisation errors and sensitive nature of using finite differences for the calculation of the Laplacian (Araujo et al. 2012). Overall this non-linear complex diffusion filter (NCDF) has been reported to give improved despeckling and denoising properties (Bernardes et al. 2010).

The NCDF method has been improved by (Bernardes et al. 2010) in their use for optical coherence tomography data for the human eye, by introducing an adaptive time step and adaptive coefficient k in Eq. (5). The reason behind an adaptive time step is due to the fact that the diffusion coefficient (Eq. 5) depends on the second order derivative of the image, which is greater during the initial steps of the diffusion process due to a greater presence of noise that is then progressively reduced; hence more emphasis has to be given to small image features during the initial iteration steps by use of small time steps initially. Choosing the correct parameter k in Eq. (5) modulates the spread of the diffusion coefficient in the vicinity of its maximum, hence at edges and homogeneous areas, where the image Laplacian disappears.

$$k = k_{MAX} + (k_{MAX} - k_{MIN}) \frac{g - \min(g)}{\max(g) - \min(g)} \tag{6}$$

where $\max(g)$ and $\min(g)$ are the maximum and minimum of g, with $g = G_{N,\sigma} * \mathrm{Re}(I)$, where $*$ is the convolution operator, $G_{N,\sigma}$ is a local Gaussian

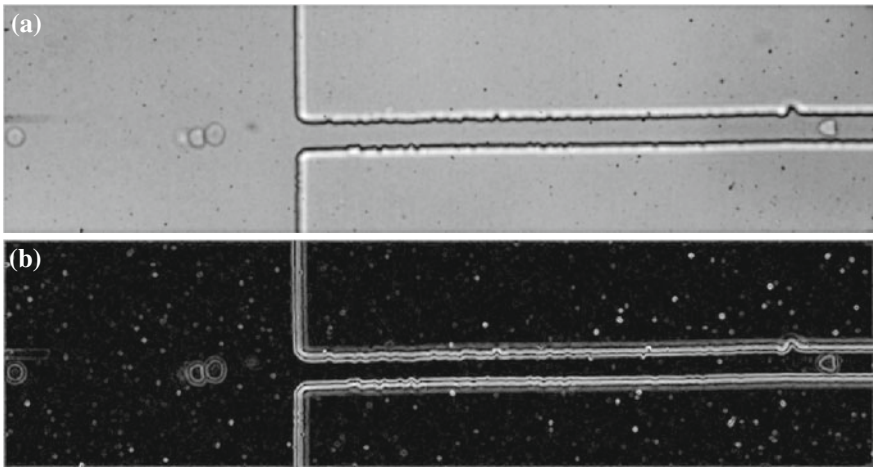

Fig. 2 Frame 50 with **a** image filtered using adaptive NCDF, **b** filtered image gradient

kernel of size $N \times N$ and standard deviation σ, and $\mathrm{Re}(I)$ denotes the real part of the image.

The adaptive time step is given by

$$\Delta t = \frac{1}{\alpha}[a + b\,\exp\{-\max(|\mathrm{Re}(\partial I/\partial t)|/\mathrm{Re}(I))\}], \tag{7}$$

where $|\mathrm{Re}(\partial I/\partial t)|/\mathrm{Re}(I)$ is the fraction of change of the image at a certain iteration step and a, b are constants and control the time step with $a + b \leq 1$. For this study $\alpha = 4$, $a = 0.25$ and $b = 0.75$ (Bernardes et al. 2010) and the result of filtering Frame 50 can be seen in Fig. 2 .

2.2 Contrast Enhancement

Even though the results obtained using the adaptive NCDF method are satisfactory due to low blurring effects (small diffusion) on the RBC edges, contrast enhancement is performed to intensify feature edges that may have been mitigated at high intensity of denoising. Here, the images have been enhanced using the *unsharp masking* method and the results are presented in Fig. 3 .

In the unsharp masking method, the enhanced image $I_{enhanced}(x, y)$ is obtained from the input image $I(x, y)$ and given by:

$$I_{enhanced}(x, y) = I(x, y) + \lambda(I(x, y) - G_\sigma * I(x, y)) = I(x, y) + \lambda F(x, y) \tag{8}$$

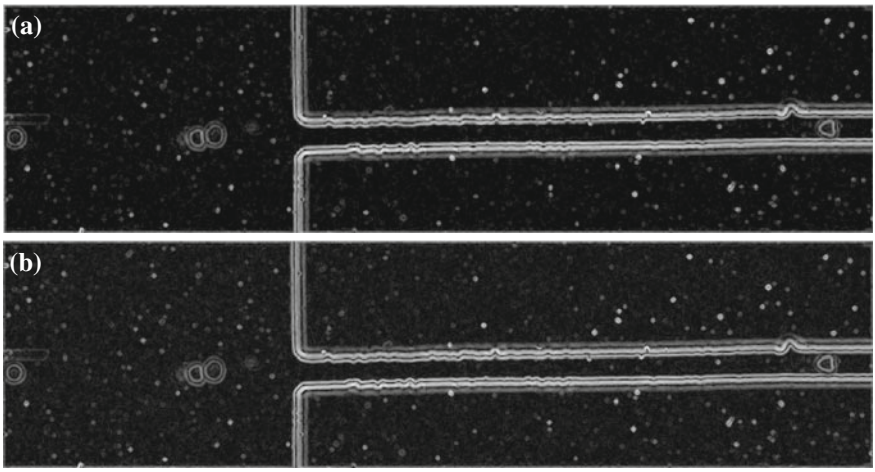

Fig. 3 Frame 50 **a** image gradient after filtering with adaptive NCDF, **b** image gradient after filtering and enhancement

where $F(x, y)$ is the correction signal computed as the output of the linear high-pass filter, and λ is the scaling factor which controls the contrast enhancement level acquired as the output image ($0 \leq \lambda \leq 1$, with $\lambda = 0.5$ throughout these results) (Polesel et al. 2000).

3 Image Quality Measures

We can now briefly compare the performance of both methods using performance metrics measures: the variance of the image pixel intensities measured locally and denoted by σ_{local}, defined by Eq. (9); and the contrast to noise ratio (CNR), defined in Eq. (10).

The local variance at a given pixel of an image is defined as

$$\sigma^2_{local}(I(x,y)) = \frac{1}{n^2} \sum_{X=-\frac{n-1}{2}}^{\frac{n-1}{2}} \sum_{Y=-\frac{n-1}{2}}^{\frac{n-1}{2}} (I(x+X, y+Y) - \mu)^2 \tag{9}$$

where μ is the mean of local region of interest of size $n \times n$, and for this work $n = 3$ was chosen. We can analyse the local variance of an image as a measure of image noise intensity, since for a binary image high values of variance are seen only at feature edges.

The CNR gives an objective measure of contrast (the difference of means) between a region of background noise (reference) and an image feature (object in study).

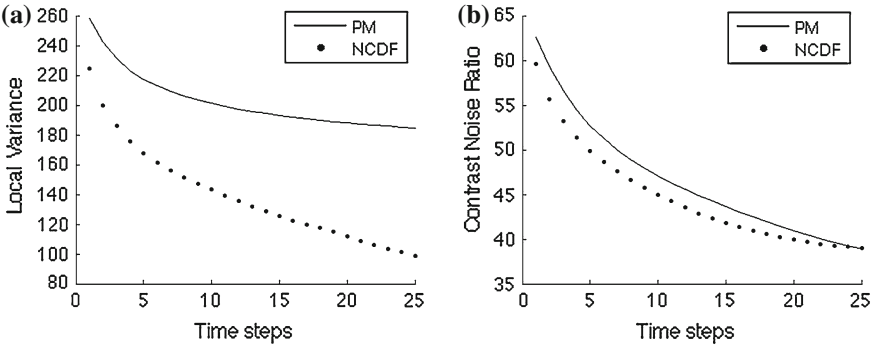

Fig. 4 Frame 50 performance metrics for filtering with: **a** average local variance of the image, **b** contrast to noise ratio

$$CNR = \frac{\mu_t - \mu_r}{\sqrt{\sigma_t^2 + \sigma_r^2}} \tag{10}$$

where μ_r and σ_r are the pixel mean and standard deviation of a reference area of the image, while μ_t and σ_t are the mean and standard deviation of the region of the object.

Fig. 4 presents the performance metrics at different levels of filtering, denoted by time evolution of Eq. (1). The mean σ^2_{local} for the image is seen to be less for the adaptive NCDF method compared to the PM method, while the CNR is comparable for both methods. Based on these results, it is apparent that the adaptive NCDF not only retain all the advantages of PM but also achieves a superior performance. A significant advantage furthermore in the adaptive NCDF method over the PM, is that the diffusion parameter need not to be defined a priori, but instead it adapts to the image in study and during the filtering process.

4 Detecting and Tracking Red Blood Cells

When tracking the RBCs in the video sequence it is often pertinent to provide information about the shape of the object. Due to the fact that cell shapes are restricted, the analysis of the image sequence can exploit the prior known information about the cells geometry in order to increase the robustness of the method and the computation time. This is moreover the case in a high frame rate video sequence, where the analysis if the previous image can be used as a starting point for the current frame.

Here two methods are presented: the Hough transform (Ballard 1981) and the Active Contours (Snakes) (Kass et al. 1988). The Hough transform is used to identify predefined shapes in a given image, here circles of integer variable radius are matched to the RBCs. The Snakes method allows for a deformable curve to

align image features, with the deformation of the curve given by a minimisation of internal (tension and bending) and external forces (image-inferred and imposed).

In the case of segmenting and tracking the RBCs, the Hough transform will only be able to provide best-fit circles, while the Snakes will be able to capture the cell deformation. The Hough transform tends to be more robust and faster as the shape is given, while the location and radius are free parameters. For the Snakes method however, there is no global structure imposed and the shape of the object is computed by local constrains of continuity and smoothness. We can argue that this makes the method more sensitive to noise and image irregularities. For both methods, the preprocessing steps of filtering and contrast enhancement considerably improve the robustness of the methods.

In this work the Hough transform is used on the first image in the sequence, and the contours provided are used to initiate the Snakes method. For the following frames in the video sequence, the RBC velocity is estimated in order to improve robustness and speed of the algorithms. Both methods are now briefly presented.

4.1 Hough Transform Method

The Hough transform method allows for object detection of a specific shape within an image that has been transformed into edge representation. In that kind of representation, sample pixels in the image do not contain the grey level information, but the magnitude and direction of the local grey level change. A commonly used edge representation is the gradient operator which provides the local grey level change as a ramp, while another possibility is the Hueckel operator which gives a step representation instead (Ballard 1981).

The basis of the general Hough algorithm used in this study is presented here concisely following the work in (Ballard 1981), and only a brief conceptual outline of the method is reported here. The gradient of the image is to infer information about object edges in the image. A threshold value for the image gradient magnitude is chosen such that pixels above this value will be considered as part of object edges. For these pixels, the gradient direction provides additional information to the edge representation. In the case of identifying circles in the image, the gradient direction will indicate the line on which the circle centre lies. An *accumulator array* is used to identify possible circle matches, and based on a scoring system the local maxima once all edge pixels have been considered, defines the circle centre and radius.

The method is robust and works well in the case of incomplete edge representations and noise, that can be handled by introducing uncertainties in the scoring system in the accumulator array. Figure 5 shows the results of RBC segmentation using Hough transform. This segmentation is used to initiate the Snakes method, by initially maintaining the centre of the identified circles but reducing the radius in order that the perimeter lies within the RBCs. The Snakes method is now briefly outlined.

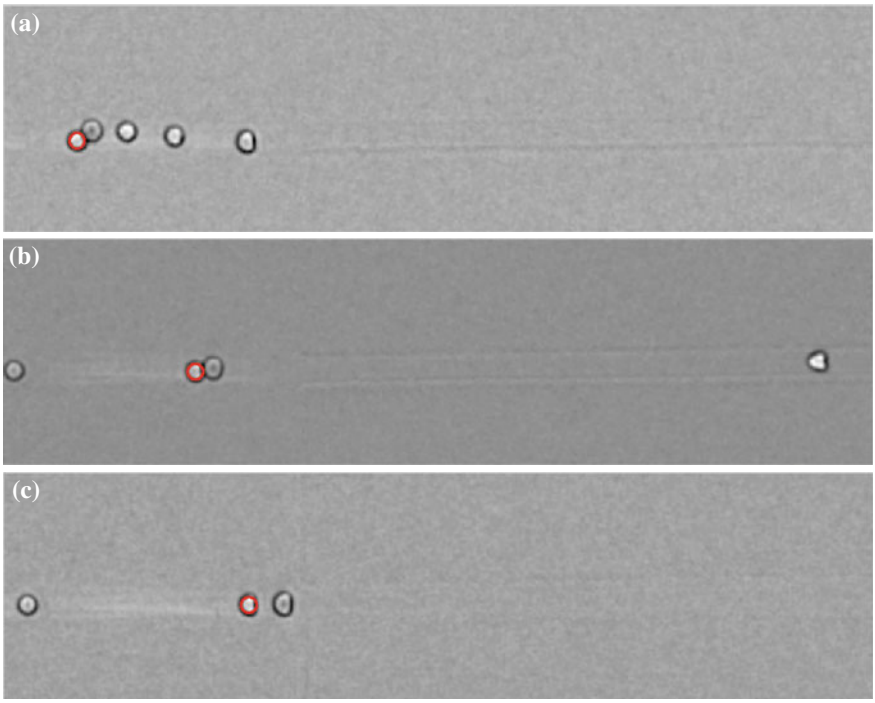

Fig. 5 Detection of one RBC in different frames using Hough transform method

4.2 Active Contours Method (Snakes)

Snakes are active contour models, which localise edges adaptively. The snake model is controlled by a continuity spline under the influence of image forces and external constraint forces, as well as internal regularising forces. The image forces push the snake toward salient image features, while the external forces are responsible for putting the snake closer to the desired local minimum (Kass et al. 1988). Here we use the slightly shrunken contour obtained using the Hough transform as the initial snake position, and allow the Snakes to adapt to the deformed RBC shape.

Considering $p(s) = (x(s), y(s))$ as the position of a Snake represented parametrically, we can write its energy functional as

$$\begin{aligned} E^*_{snake} &= \int_0^1 E_{snake}(p(s))\, ds \\ &= \int_0^1 E_{internal}(p(s)) + E_{external}(p(s))\, ds \end{aligned} \tag{11}$$

where $E_{internal}$ is the internal energy due to tension and bending, and $E_{external}$ is given by the summation of the image forces E_{image} with the constraint forces E_{constr} (Kass et al. 1988), hence $E_{external} = E_{image} + E_{constr}$.

The internal spline energy of the Snake is given by a first-order term controlled by $\alpha(s)$, and second-order term controlled by $\beta(s)$ and can be written as

$$E_{internal} = \frac{1}{2}(\alpha(s)|p_s(s)|^2 + \beta(s)|p_{ss}(s)|^2) \tag{12}$$

The first-order term weighted by $\alpha(s)$ regulates the membrane behaviour (tension), while the second-order term weighted by $\beta(s)$ regulates the thin-plate behaviour (bending).

To make sure that the external energy attracts the snakes to salient features of the image, three different energy functions are used for E_{image}, given by a weighted combination of the functionals that attract the Snake to lines, edges and terminations:

$$E_{image} = w_{line}E_{line} + w_{edge}E_{edge} + w_{ter}E_{ter} \tag{13}$$

The different behaviours of the snake are adjusted by the weights w_{line}, w_{edge} and w_{ter}. The most commonly used image functional is the image intensity, hence $E_{line} = I(x, y)$. Depending on the sign of w_{line}. The Snake is attracted either to light or dark lines. The edge functional allows the Snake to be attracted to contours with large image gradients and is commonly given by $E_{edge} = -|\nabla I(x, y)|^2$. The termination functional E_{ter} permits the Snake to be attracted to terminations (corners) by using the curvature of level lines. The curvature of a contour in a two-dimension image is given by:

$$E_{ter} = \frac{C_{yy}C_x^2 - 2C_{xy}C_xC_y + C_{xx}C_y^2}{(C_x^2 + C_y^2)^{3/2}} \tag{14}$$

where $C(x, y) = G_\sigma(x, y) * I(x, y)$, and $G_\sigma(x, y)$ is a Gaussian of standard deviation σ. The constraint forces E_{constr} is used to define attractive (or repulsive) forces, that can be denied manually or automatically. Here $E_{constr} = k/(|\mathbf{q} - \mathbf{x}|^2)$, as a repulsive force located at position $\mathbf{q}$, which is the centre of the closed contour from the previous frame that has been shrunk to fit inside the RBC. In this way E_{constr} serves as an inflation force to push the Snake out.

Different weights in the energy functionals give different properties to the Snake and the interpretation of the image information. Figure 6 shows the results for different images in the stack, tracking a single RBC.

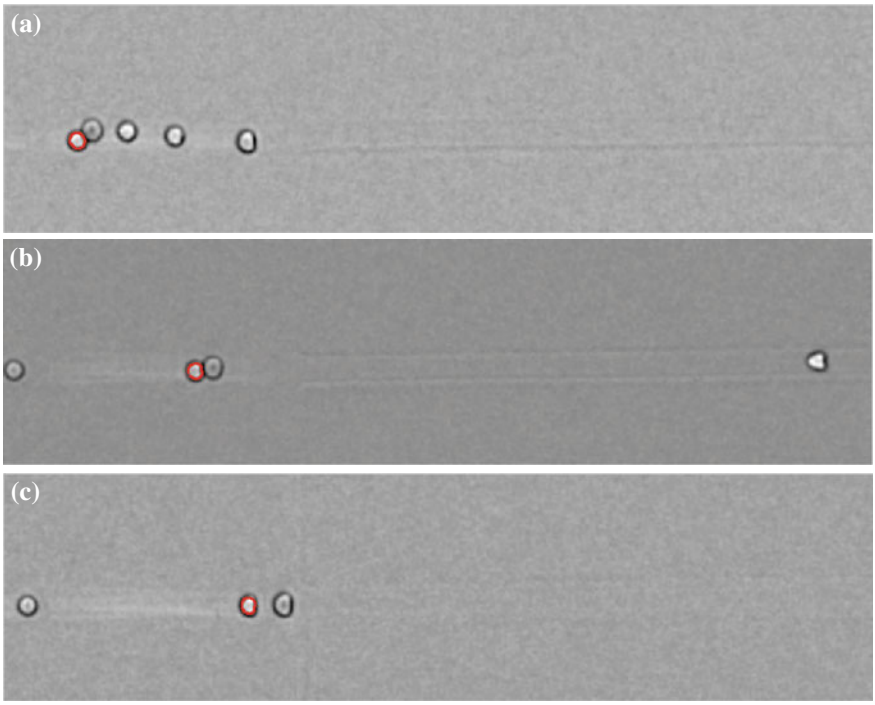

Fig. 6 Detection of one RBC in different frames using our algorithm

4.3 Outline of Algorithm

The algorithm is concisely presented in Fig. 1. The image processing steps are in order: (1) subtract the image stack average from each image; (2) perform filtering using the adaptive NCDF method; (3) perform contrast enhancement using the unsharp masking method. From here the first frame in the sequence is taken and the Hough transform is used to identify the best-fit circles to the RBCs. These are shrunk to fit entirely within each RBC and then the Snakes method is used to capture the RBC shape more accurately. For subsequent frames, each RBC velocity is estimated, the contour from the previous frame is translated accordingly and shrunk slightly to ensure that the contour lies within the RBC, and the Snakes method is used again to identify delineate the RBCs. This is continues until all frames in the video sequence have been analysed.

In the experimental data studied, the micro-channel is not deep such that RBCs will not move entirely out of the focusing plane. This signifies that no RBC will appear or disappear within the domain but only enter or leave through the inflow and outflow edges, respectively. In the case of different setups where the channel height is greater to allow RBC to move in and out of the focal plane, and in the case of tracking newly entering RBCs, the Hough transform can be used more

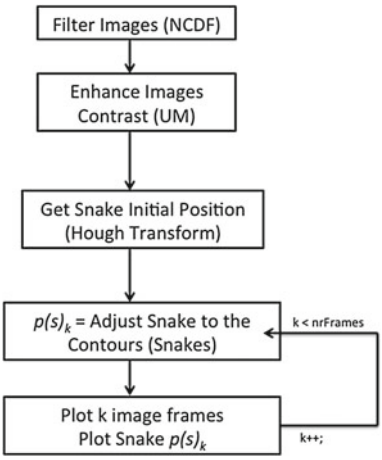

Fig. 7 RBC detection algorithm

regularly in the image stack to identify the RBCs and not track them, as mentioned above, with an added computational cost.

Tracking is possible by considering the centre and radius of each RBC, detecting the closest ones in adjacent frames in the image stack. The RBC perimeter is discretised parametrically in the Snakes method into straight line segments. The contour thus represented, is used to calculate the centroid of the polygon and its area. Let us consider our contour as a non-self-intersecting closed polygon defined by M vertices $(x_0, y_0), (x_1, y_1), \ldots (x_M, y_M)$, the centroid is the pixel C_x, C_y where

$$\begin{aligned} C_x &= \frac{1}{6A} \sum_{i=0}^{M-1} (x_i + x_{i+1})(x_i y_{i+1} - x_{i+1} y_i) \\ C_y &= \frac{1}{6A} \sum_{i=0}^{M-1} (y_i + y_{i+1})(x_i y_{i+1} - x_{i+1} y_i) \end{aligned} \tag{15}$$

where A is the contour area given by $A = \frac{1}{2} \sum_{i=0}^{M-1} (x_i y_{i+1} - x_{i+1} y_i)$. The vertices are numbered in order of their occurrence along the contour's perimeter, and the last vertex (x_M, y_M) is assumed to be the same as the first one (x_0, y_0). We should note that if the vertices are numbered clockwise the area A will have a negative value, but the centre coordinates will still be correct.

The method is fully automatic, robust, fast and accurate enough for the purpose of identifying, tracking and analysing the shapes of the RBCs. An example of tracking a RBC is shown in Fig. 8.

Results are shown in Fig. 9 for the tracking of a RBC undergoing large deformations (Table 1). From this figure it is evident that the outlined method proves to be sufficiently robust in the cases of: a rounded shape RBC, slightly deformed, and severely deformed by the channel.

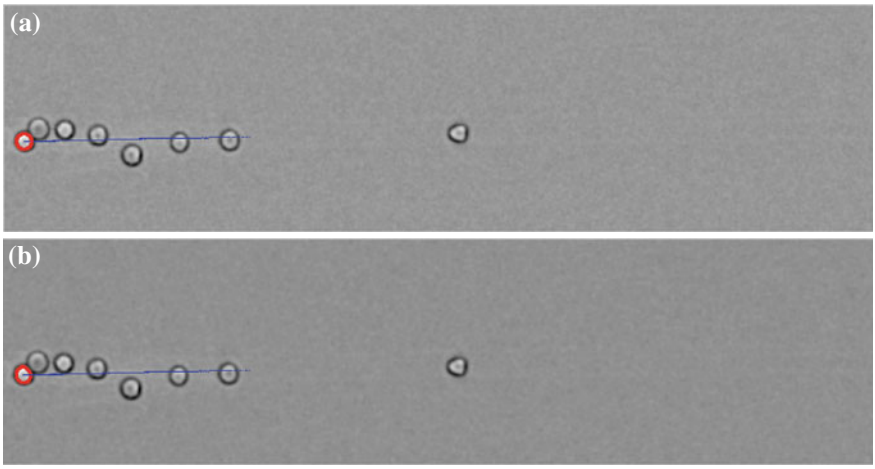

Fig. 8 Tracking an RBC using the **a** Hough transform and **b** Snakes

Table 1 RBC deformation at different regions of the PDMS micro-channel (in pixels)

	RBC perimeter			RBC area		
	Region 1	Region 2	Region 3	Region 1	Region 2	Region 3
Hough	43.9823			153.9380		
Hough + Snakes	46.1460	45.0526	47.4106	179.2320	175.4701	178.2284

5 Results and Discussion

A method for identifying and tracking red blood cells from experimental data has been put forward. The analysis of the translation and deformation of the RBCs is now discussed in terms of basic measures such as the perimeter length and the area. Comparison is performed on the filtering methods (PM and adaptive NCDF) as well as the segmentation methods (Hough transform and Snakes) in order to investigate suitability and give an indication of errors or variability that the analysis is susceptible to.

Initially we focus on testing the filtering method used, hence the anisotropic diffusion presented in Eq. (1) for both diffusivity coefficients: the gradient based function in Eq. (2) (Perona and Malik 1990), and the Laplacian based coefficient from Eq. (5) together with the adaptivity methods of Eqs. (6, 7) (Bernardes et al. 2010). Results are shown in Fig. 4 for measures of the mean local variance (Eq. 9) and contrast to noise ration (CNR) (Eq. 10). As noted above, this result indicates that improved noise removal is obtained with no effective loss in the CNR, leading to the proposition that adaptive NCDF performs better than PM methods for the data case used in this work.

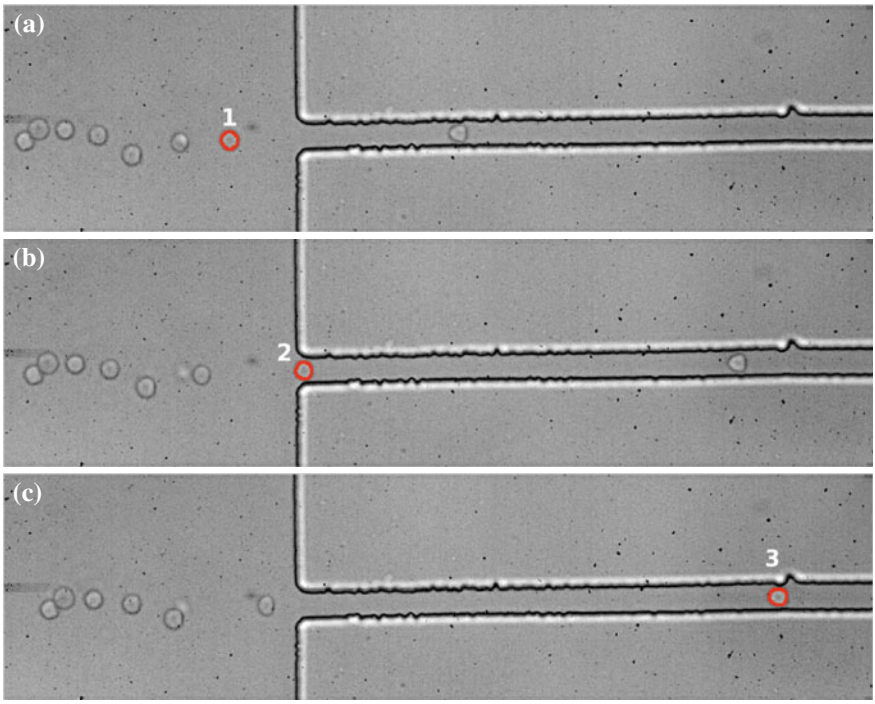

Fig. 9 RBC deformation in different regions of the PDMS micro-channel **a** region with no contraction, **b** beginning of the micro-channel, **c** narrow region of the micro-channel

The effect of filtering and enhancing the contrast is complemented with results presented in (Fig. 10). These show the variation of image intensity and intensity gradient along a line. As expected, filtering the image alters significantly the quality by reducing noise, and subsequently leading to a more accurate and robust segmentation and subsequent analysis.

We now observe the effects of the segmentation methods with respect to basic shape measures. The RBCs were analysed in three frames of the sequence, indicated by (1), (2) and (3) in Fig. 9. Location (1) is in a region of free flow before the contraction, (2) is at the beginning of the micro-channel constriction, and (3) is within the constriction. Results are presented in Table 1. Far from the contraction region, the red blood cells are effectively circular, resulting in a bigger area as it lies largely in the focus plane. The deformation index (ratio between the major and minor axes of an ellipse that best fits the RBC) will hence give values close to unity. As the cells approach the contraction, location (2), and during the contraction itself, location (3), they become deformed with an elongated shape. Due to the RBC deformation in the contraction, the RBC perimeter increases as well as the deformation index. This occurs since the cells are being submitted to strong shear flow.

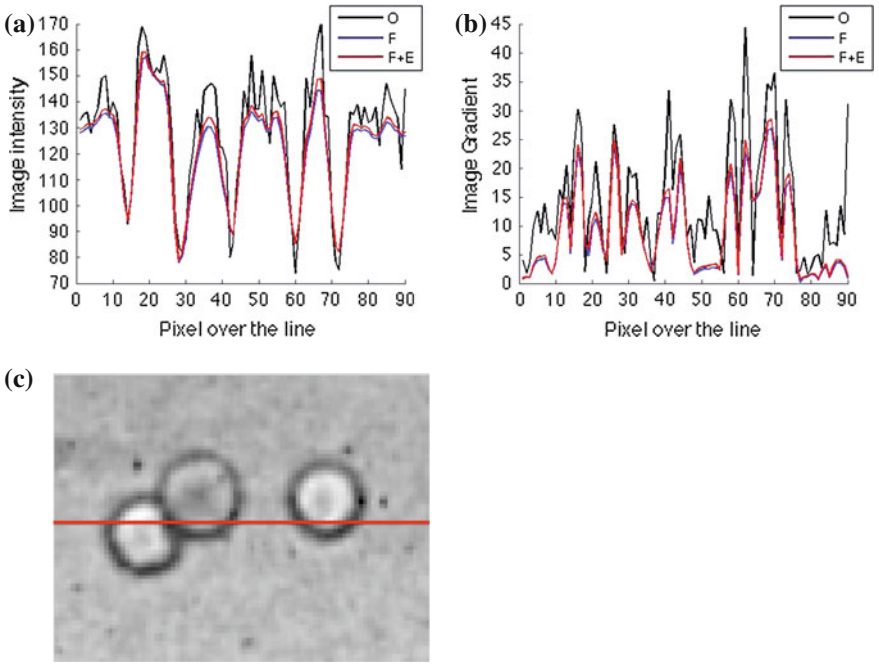

Fig. 10 Variation of image intensity (**a**) and intensity gradient (**b**), along a *red line* (from *left* to *right*) shown in (**c**). Key: *O* Original; *F* Filtered (using adaptive NCDF); $F + E$ Filtered and Enhanced (using unsharp masking)

Results have shown the potential advantage of using preprocessing techniques in image segmentation, which was one of our goals during this study. When considering RBC deformation, in order to deeply understand the findings, tests have to be done with different concentration of RBCs (hematocrit) and flow rates as well as different geometries of the micro-channel. The results show that the RBCs are highly deformable under strong shear flows. Different hematocrit levels or flow rates will provide further results, such as the influence and size of the cell-depleted regions near the stationary walls, and effects non-Newtonian rheology in small vessels.

Acknowledgments The authors kindly acknowledge the support provided by CEMAT/IST and funding support by the FCT project BIOMIMETIC—PTDC/SAU-ENB/116929/2010. We kindly thank Prof. Rui Lima and his research team from Instituto Politécnico de Bragança, and Prof. Takami Yamaguchi and his research team from Tohoku University, for providing the experimental data.

References

Araujo A, Barbeiro A, Serranho P (2012) Stability of finite difference schemes for complex diffusion processes. SIAM J Numer Anal 50(30):1284–1296

Ballard DH (1981) Generalizing the Hough transform to detect arbitrary shapes. Pattern Recogn 13(2):111–112

Bernardes R, Maduro C, Serranho P, Araujo A, Barbeiro S, Cunha-Vaz J (2010) Improved adaptive complex diffusion despeckling filter. Opt Express 18(23):24048–24059

Fung Y, Perrone N, Anliker M (1970) Biomechanics: its foundation and objectives. Prentice-Hall, Englewood Cliffs

Gilboa G, Sochen N, Zeevi YY (2004) Image enhancement and denoising by complex diffusion processes. IEEE Trans Pattern Anal Mach Intell 26(8):1020–1036

Guidotti P (2012) A family of nonlinear diffusions connecting perona-malik to standard diffusion. Discrete Contin Dyn Syst Ser S 5(3):581–590

Hou, Han Wei, Bhagat, ALI Asgar S, Lin Chong, AlvinGuo, Mao, Pan, Wei Tan, Kevin Shyong, Han, Jongyoon Lim, Chwee Teck (2010) Deformability based cell margination-a simple microfluidic design for malaria-infected erythrocyte separation. Lab Chip 10:2605–2613

Kass M, Witkin A, Terzopoulos D (1988) Snakes: active contour models. Int J Comput Vision 1(4):321–331

Mohandas N, Evans E (1994) Mechanical properties of the red cell membrane in relation to molecular structure and genetic defects. Annu Rev Biophys Biomol Struct 23:787–818

Musielak M (2009) Red blood cell-deformability measurement: review of techniques. Clin Hemorheol Microcirc 42(1):47–64

Perona P, Malik J (1990) Scale-space and edge detection using anisotropic diffusion. IEEE Trans Pattern Anal Mach Intell 12(7):629–639

Polesel A, Ramponi G, Mathews VJ (2000) Image enhancement via adaptive unsharp masking. IEEE Trans Image Process 9(3):505–510

Salinas HM, Fernandez DC (2007) Comparison of pde-based nonlinear diffusion approaches for image, enhancement and denoising in optical coherence tomography. IEEE Trans Med Imag 26(6):761–771